*Journal of Alloys and Compounds, 182* (1992) 211–221
*JALCOM 162*



# Coercivity through controlled crystallization in melt-spun Nd–Fe–B amorphous alloys

M. T. Clavaguera-Mora, J. A. Diego, M. D. Baró and S. Suriñach
*Física de Materials, Departament de Física, Universitat Autònoma de Barcelona, 08193-Bellaterra (Spain)*

N. Clavaguera
*Departament d'Estructura i Constituents de la Matèria, Facultat de Física, Universitat de Barcelona, Diagonal 647, 08028-Barcelona (Spain)*

J. M. González and F. Cebollada
*Instituto de Ciencia de Materiales, Serrano 144, 28006-Madrid (Spain)*

(Received July 25, 1991; in final form October 28, 1991)

## Abstract

The kinetics of crystallization of amorphous melt-spun $Nd_{13}Fe_{79}B_8$ alloy induced by thermal treatment was studied by differential scanning calorimetry, scanning and transmission electron microscopy and magnetic measurements. The optimization of coercivity through controlled crystallization is explained as a consequence of the crystallization kinetic behaviour. Optimal materials are obtained by annealing the amorphous alloys at temperatures in the range 950–1000 K for times of the order of 15 min. After that heat treatment a fully crystallized material is obtained with a mean grain size of about 60 nm and a coercivity of 1.4 T.

## 1. Introduction

Commercial Nd–Fe–B permanent magnetic materials are usually prepared by either sintering or rapid quenching [1–4]. The microstructures of the magnets produced by the latter technique have received considerable attention [5–9], but relatively little is known about the kinetics of crystallization and its significance in the microstructure and magnetic properties. The magnetic properties of melt-spun ribbons of a given composition depend on the quench rate and on the heat treatment [10–14]. The relationship between the quench rate and the grain size has already been established [7, 9] and coercivities up to 1.4 T can be obtained in these materials by heat treatment.

In this paper a detailed investigation of the kinetics of crystallization of amorphous alloys produced by the melt-spinning technique is discussed. The importance of controlling the kinetics to produce hard magnetic materials is demonstrated by a study of the influence of the heat treatment on the microstructure and coercivity.

0925-8388/92/$5.00
© 1992 – Elsevier Sequoia. All rights reserved

## 2. Experimental procedure

Master alloys of $Nd_{13}Fe_{79}B_8$ were provided by Gesellschaft für Elektrometallurgie, Nürnberg and their microstructure was characterized by optical and scanning electron microscopy. Melt-spun alloys were obtained by quenching the molten material on the surface of a rapidly spinning (about 40 m $s^{-1}$) copper wheel under a helium atmosphere. X-ray diffraction, transmission electron microscopy (TEM) and measurement of the hysteresis loop confirmed the amorphous state of the melt-spun alloys.

Differential scanning calorimetry (DSC) measurements were performed in a computerized Perkin–Elmer DSC-II instrument in both isothermal and continuous heating regimes on the melt-spun ribbons (for more details see ref. 15). To analyse the crystallization kinetics, both the crystallized fraction $x$ and the transformation rate $dx/dt$ at a given time $t$ or temperature $T$ were determined following the current procedure [16].

Microstructural observations were carried out on thin foils prepared by ion beam milling with a TEM Hitachi H-880 (200 kV). These measurements were complemented by optical microscopy and scanning electron microscopy (SEM) observations.

Magnetic measurements were carried out on samples prepared from finely crushed flakes of melt-spun and heat-treated material mixed with an inorganic vitreous binder (sodium silicate). Samples were formed by cold pressing (200 MPa) this mix to a cylindrical shape (2 mm height, 3 mm diameter). Hysteresis properties were measured up to a maximum field $\mu_0 H = 4$ T by using an extraction device.

## 3. Results and discussion

### *3.1. Characterization of the master alloy*

Figure 1 shows the microstructure of the master alloy observed by SEM. It is possible to see that the majority of the crystals are of the hard magnetic $\Phi$ phase ($Nd_2Fe_{14}B$) as expected. Sometimes a dendritic iron nucleus appears inside the $\Phi$ crystals (A and B), while in general these crystals grow without iron inside them (C). In the gaps between the $\Phi$ crystals two other phases are present: small $\eta$ plates ($Nd_1Fe_4B_4$) attached to the crystals (D) and a neodymium-rich phase filling the rest of the gap (E). This microstructure agrees with the equilibrium phase diagram of the system [17].

### *3.2. Calorimetric behaviour*

Four exothermic crystallization peaks appear on heating the amorphous material and sometimes they are rather overlapped. In Fig. 2 the DSC curve (at a heating rate of 40 K $min^{-1}$) of the amorphous alloy (a) is compared with that of the same alloy previously annealed at 810 K for 1 h (b). During the isothermal anneal at 810 K the first two crystallization peaks are activated and, as seen in Fig. 2(b), on heating this partially crystalline sample, only

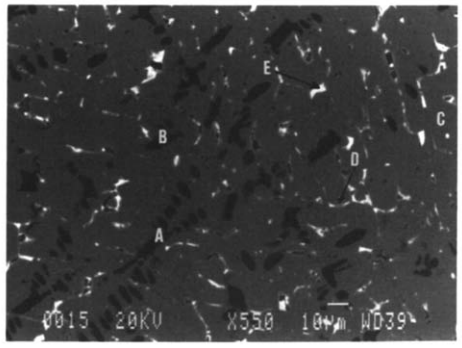


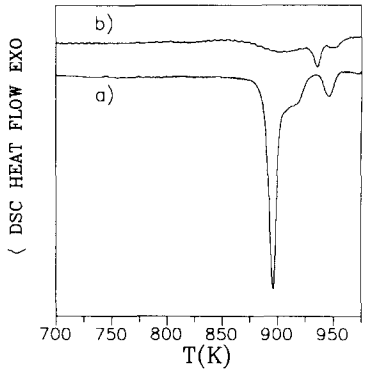


Fig. 1. Scanning electron micrograph of as-cast $Nd_{13}Fe_{79}B_8$: A, B, dendritic iron nuclei; C, hard magnetic $\Phi$ phase; D, $\eta$ plates; E, neodymium-rich phase.

Fig. 2. DSC curves at a heating rate of 40 K $min^{-1}$ of (a) an amorphous ribbon and (b) after annealing it at 810 K for 1 h.

the remaining peaks appear in the DSC curve. The general form of the exothermic peaks agrees with that published for melt-spun alloys of similar composition.

*3.3. Kinetics of crystallization*

To study the crystallization kinetics, we assume, as is often the case, that each crystallization exotherm follows a general equation of the form

$$\frac{dx}{dt} = K(T) f(x) \tag{1}$$

where the rate constant $K(T)$ shows an Arrhenius behaviour

$$K(T) = K_0 \exp\left(-\frac{E}{RT}\right) \tag{2}$$

where $E$ is the apparent activation energy and $K_0$ is the pre-exponential factor. Under constant-heating-rate ($\beta$) conditions this equation can be integrated to give

$$g(x) = \int \frac{dx}{f(x)} = \frac{K_0}{\beta} \int \exp\left(-\frac{E}{RT}\right) dT \tag{3}$$

or under isothermal conditions

$$g(x) = \int \frac{dx}{f(x)} = K(T)\, t \tag{4}$$

Since the crystallization peaks are somewhat overlapping, as seen in Fig. 2, the first and second crystallization peaks were treated as a single process and the same was done with the third and fourth peaks. This was possible because of the very similar values of the apparent activation energy of each pair of processes [15].

*3.4. Determination of the T–T–T and T–HR–T curves*

The DSC technique is a very powerful tool for determining the classical time–temperature transformation (T–T–T) curve. Effectively, eqn. (4), when represented as the temperature *vs.* the time needed to crystallize a fixed fraction $x$ of material, gives the T–T–T curve. In so far as the kinetic parameters are known, we can construct the T–T–T curves for the various processes. This has been done and the curves obtained are plotted in Fig. 3. The two bottom curves represent the time–temperature at which 10% and 90% of the first two crystallization peaks have proceeded. In a similar way the top two curves represent the time–temperature at which 10% and 90% of the third and fourth crystallization peaks have proceeded. Because of the assumptions inherent in this approach [15], we cannot extend the validity of the treatment to high temperatures. With that limitation the curves plotted in Fig. 3 are good estimates of the low temperature part of the T–T–T curves. They are important because they show that the last exothermic peaks can only be achieved at typical annealing times less than $10^4$ s if the annealing temperature is higher than about 880 K.

One can argue that in practice it is not possible to reach elevated temperature instantaneously; therefore it should be of interest to know how the different crystallization processes will take place when the glass is submitted to a constant heating rate. It is possible to construct what we call a 'temperature–heating rate transformation' (T–HR–T) curve, which represents the temperature at which a certain amount of crystalline material will be present on heating as a function of the heating rate [18]. Such a representation can be obtained by solving eqn. (3). The results obtained are shown in Fig. 4. Curves $a_1$ and $a_2$ ($b_1$ and $b_2$) represent the loci of the points where 10% and 90% of the first and second (third and fourth) crystallization processes are achieved.

This figure reflects the difficulty in obtaining a fully crystallized material by heating the amorphous ribbon to moderate temperatures. The important point is that even when very low heating rates (about 1 K $min^{-1}$) are applied, it is necessary to proceed up to temperatures above about 910 K in order that the last two stages of crystallization take place.

*3.5. Microstructural investigation*

Systematic microstructural observations made by SEM [19] showed that, irrespective of the heat treatment, the microstructure of the crystallized material is refined from the wheel surface (crystallite size about 200 nm) towards the free surface (size about 50 nm). Other authors [20, 21], using argon as the inert gas atmosphere in the melt-spinning process, found that the finest microstructure of partially crystalline ribbons quenched at a wheel speed of 20 m $s^{-1}$ is formed on the wheel side of the ribbon. Variables other than the wheel speed and the environmental gas may also be related to the different behaviour observed.

TEM observations show that the grain boundary phase appears partially amorphous when the annealing temperature is in the range 780–830 K.

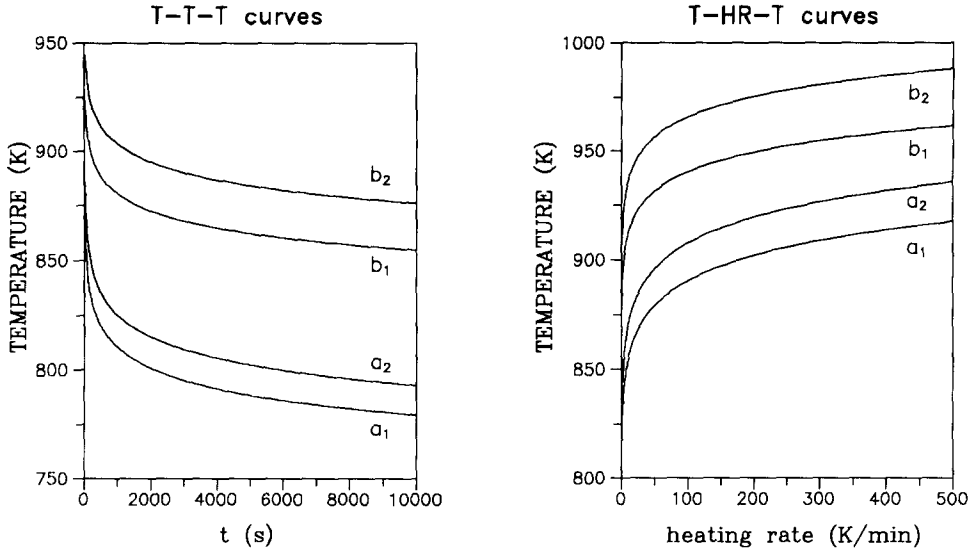


Fig. 3. Time–temperature transformation (T–T–T) curves for $Nd_{13}Fe_{79}B_8$ alloy. Curves $a_1$ ($b_1$) and $a_2$ ($b_2$) correspond to a crystalline fraction of 0.1 and 0.9 respectively of the total transformation occurring in the first (second) crystallization step.

Fig. 4. Temperature–heating rate transformation (T–HR–T) curves for $Nd_{13}Fe_{79}B_8$ alloy. Curves $a_1$ ($b_1$) and $a_2$ ($b_2$) correspond to a crystalline fraction of 0.1 and 0.9 respectively of the total transformation occurring in the first (second) crystallization step.

Typical micrographs are shown in Figs. 5–7. The progress of crystallization on annealing the melt-spun ribbon at 810 K is shown in Fig. 5. The first crystalline grains are seen after 10 min annealing (Fig. 5A). Nucleation and growth continue with further annealing as shown in Figs. 5B–5D, which correspond to annealing times of 30, 45 and 75 min respectively. For long annealing times the crystalline grains are embedded in a still amorphous matrix. The presence of an amorphous phase at the boundary between grains is better seen in Fig. 6, which shows the microstructure of a melt-spun ribbon annealed for 45 min at 810 K. Diffraction from these films is not possible owing to the interference from the adjacent grains [6]. Figure 7 shows the microstructure of ribbons which were annealed for 15 min at 1000 K. The crystallites are similar in size to those obtained when annealing at 810 K but no trace of grain boundary amorphous phase could be seen. They have a perfect crystalline structure, which is indicated by the moiré patterns produced when the grains overlap.

To further elucidate the influence of the heat treatment on the microstructure, the melt-spun amorphous alloy was subjected to two different annealing conditions: (a) a long-term anneal of about 5 h (or about 2 h) at a low temperature of 780 K (or 810 K) followed by an anneal of 15 min at 950 K; (b) a short-term anneal of 15 min at 950 K. No significant difference

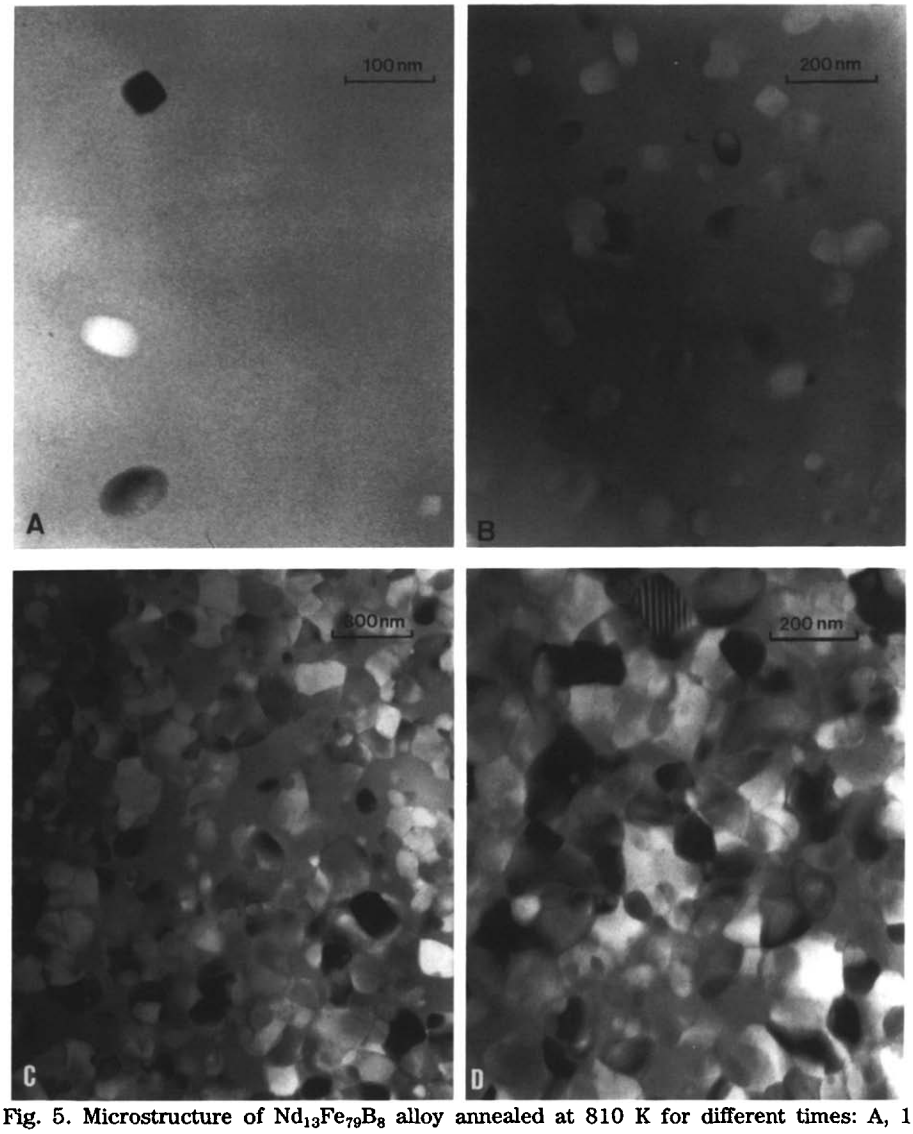


Fig. 5. Microstructure of $Nd_{13}Fe_{79}B_8$ alloy annealed at 810 K for different times: A, 10; B, 30; C, 45; D, 75 min.

in the microstructure is observed when the samples are annealed at 780 K for 5 h 15 min or at 810 K for 2 h 15 min and then annealed for 15 min at 950 K. However, a refinement in microstructure is observed when the sample is heated to 950 K at 320 K $min^{-1}$ and annealed for 15 min at this temperature. Figures 8(A) and 8(B) show that the typical size of crystals in the centre of the ribbon changes from 200 nm for long-term annealed samples to 60 nm for short-term annealed ones.

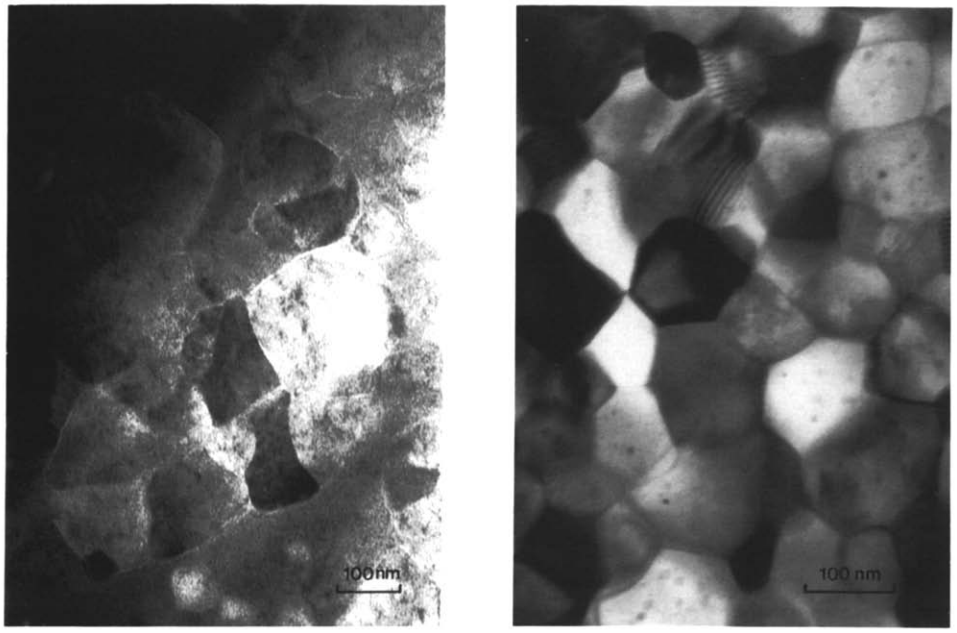


Fig. 6. Microstructure of melt-spun $Nd_{13}Fe_{79}B_8$ alloy after annealing at 810 K for 45 min.

Fig. 7. Microstructure of melt spun $Nd_{13}Fe_{79}B_8$ alloy after annealing at 1000 K for 15 min.

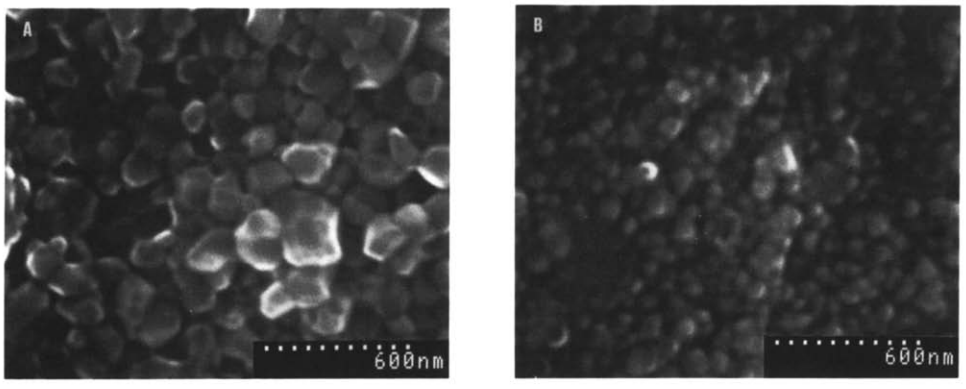


Fig. 8. Scanning electron micrographs of melt-spun $Nd_{13}Fe_{79}B_8$ alloy (centre of ribbon) after (A) a long-term anneal at 810 K for 2 h 15 min and then further annealed at 950 K for 15 min and (B) heating to 950 K at 320 K $min^{-1}$ and then annealing at this temperature for 15 min.

### *3.6. Magnetic measurements*

In order to get an adequate description of the behaviour of multiphase samples, the coercive field of the different phases was evaluated as corresponding to the different maxima in the susceptibility along the demagnetizing curve (instead of using the condition $M = 0$, which may induce error in this kind of sample).

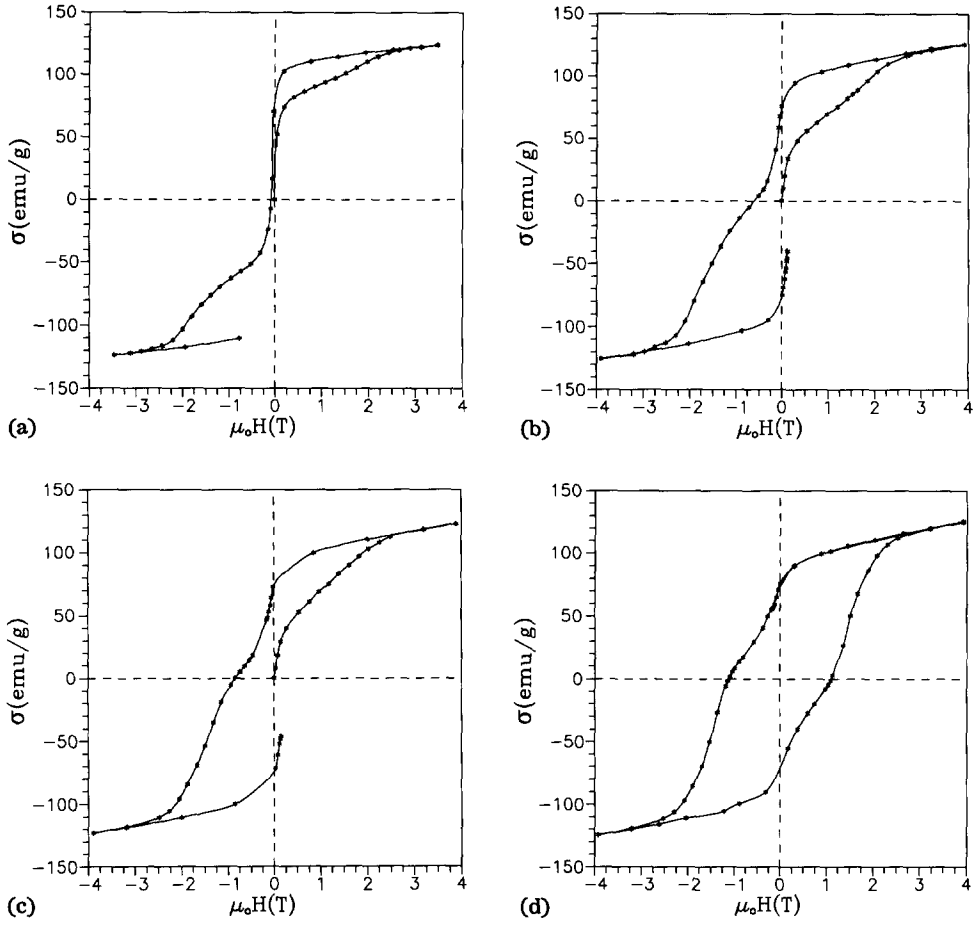


Fig. 9. Initial magnetization curve and upper branch of hysteresis loop of samples annealed at 810 K for (a) 10, (b) 30 and (c) 45 min. (d) Hysteresis loop of a sample annealed at 810 K for 75 min.

As a general feature, it is worth mentioning that a similar dependence of the coercive field (measured in minor loops) on the maximum applied field was observed in all the samples: after an initial increase to values below 0.2 T, a region of slow increase extended up to a step-like increase which ranged close to the (saturation) coercive force.

In Figs. 9–11 we present results illustrating the influence on the hysteresis behaviour of different thermal treatments leading to partial and full crystallization of the melt-spun samples. Figure 9 shows (together with the virgin curve) the upper branch of the hysteresis loop of samples annealed at 810 K for 10, 30, 45 and 75 min. As previously discussed (Fig. 2), these treatments correspond to the progress of the crystallization phenomena associated with the first two exothermic peaks; that is, basically, to the appearance of the

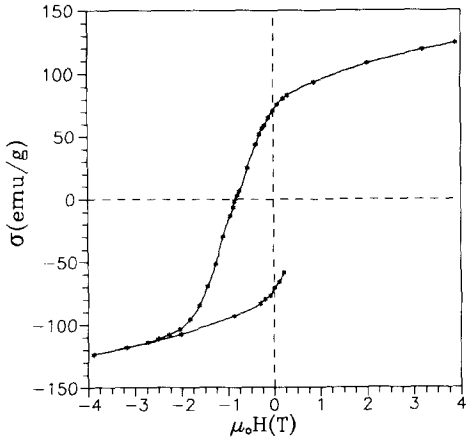


Fig. 10. Upper branch of hysteresis loop of a sample annealed first at 810 K for 75 min and then at 1000 K for 15 min.

hard magnetic phase. The progress of crystallization was also visualized microscopically in Fig. 5. From the shape of the demagnetizing curves the coexistence in the samples of at least two magnetic phases is clear: a soft phase with a coercive force $\mu_0 H_1 = 0.15$ T and a hard phase which is demagnetized in the third quadrant and has a coercive force $\mu_0 H_2 = 1.35$ T. We identify the initial step decay of the magnetization (upon applying negative fields) with the demagnetization of the remaining portion of the amorphous phase, although this part of the curves should also include a contribution from a small number of $\alpha$-Fe crystallites detected by X-rays in the heat-treated samples.

Figure 10 corresponds to the results obtained for a sample first annealed at 810 K for 75 min and then annealed at 1000 K for 15 min to get full crystallization. The linear-like shape of the demagnetizing curve is apparent in this case, indicating the high degree of inhomogeneity in the microstructure of the sample (see Fig. 8). Also, a decrease in the coercive force, $\mu_0 H_c = 1.0$ T, was observed.

Finally, in Fig. 11 we present the results corresponding to samples annealed for 15 min at 900, 950 and 1000 K to get full crystallization. No soft phases are observable and so a smooth demagnetizing curve was measured. In these samples the coercive force $\mu_0 H_c = 1.4$ T coincides with the condition $M = 0$ and, comparing Figs. 9 and 11, we can see that optimum magnetic properties are associated with crystallization at high temperature. This result can be related to the achievement by this treatment of a microstructure characterized by a sufficiently small and homogeneous grain size of the hard phase as seen in Fig. 8(B), a smooth grain surface of these hard phase grains and, more importantly, a structure of secondary phases that minimizes coupling between these hard phase grains.

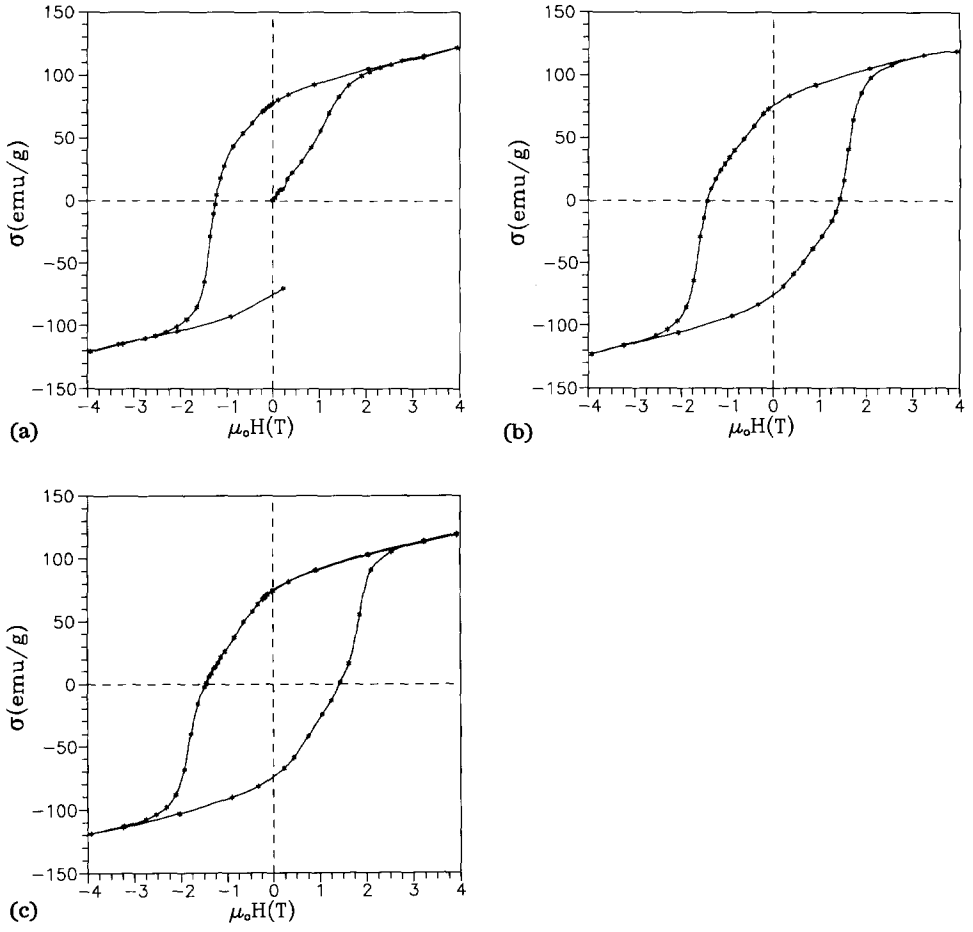


Fig. 11. Initial magnetization curve and upper branch of hysteresis loop for a sample annealed for 15 min at 900 K (a). Hysteresis loops of samples annealed for 15 min at (b) 950 and (c) 1000 K.

## 4. Conclusions

The optimization of coercivity through controlled crystallization in melt-spun Nd–Fe–B amorphous alloys can be explained by the peculiar crystallization kinetics and microstructure of the several phases present in the crystallized material. Crystallization proceeds in four steps. The first two steps can be activated either by isothermal annealing at temperatures typically in the range 800–830 K if annealing times in the range 500–5000 s are used, or by continuous heating up to temperatures below 900 K if heating rates less than 100 K $min^{-1}$ are used. The last two steps can only be activated either by isothermal annealing or by continuous heating at temperatures above about 880 K. The low temperature parts of both the T–T–T and

T–HR–T curves have been constructed in order to determine the suitable heat treatment for this material.

TEM analysis showed that once the first two crystallization processes have proceeded, the crystalline grains are still embedded in an amorphous matrix. The hysteresis loop of the partially crystalline samples shows the coexistence of a soft and a hard magnetic phase. No trace of amorphous phase appears after annealing at 900–1000 K. The fully crystalline samples show a coercivity which depends on the heat treatment: samples first heat treated at 810 K and subsequently annealed at 1000 K have lower coercivity values than those directly annealed at 1000 K, probably because in the latter either the total amount of $\Phi$ phase is larger (less $\alpha$-Fe and $Nd_{1+\epsilon}Fe_4B_4$) or there is a higher degree of homogeneity in the structure.

## Acknowledgments

This work was partially supported by EURAM (contract MA1E.0061.C(H)), CYCIT (project MAT88-0314) and CIRIT (project AR90/3-640), all of which are acknowledged.

## References

1 M. Sagawa, S. Fujimura, N. Togawa, H. Yamamoto and Y. Matsuura, *J. Appl. Phys.*, *55* (1984) 2083.
2 J. J. Croat, J. F. Herbst, R. W. Lee and F. E. Pinkerton, *J. Appl. Phys.*, *55* (1984) 2078.
3 Y. F. Tao and G. C. Hadjipanayis, *J. Appl. Phys.*, *57* (1985) 4103.
4 K. H. J. Buschow, *Mater. Sci. Rep.*, *1* (1986) 1.
5 G. C. Hadjipanayis, K. R. Lawless and R. C. Dickerson, *J. Appl. Phys.*, *57* (1985) 4097.
6 R. K. Misra, *J. Magn. Magn. Mater.*, *54–57* (1986) 450.
7 R. Coehoorn and J. Duchateau, *Mater. Sci. Eng.*, *99* (1988) 131.
8 G. C. Hadjipanayis, in M. D. Baró and N. Clavaguera (eds.), *Current Topics on Non Crystalline Solids*, World Scientific, Singapore, 1986, p. 53.
9 G. E. Carr, H. A. Davies and R. A. Buckley, *Mater. Sci. Eng.*, *99* (1988) 147.
10 J. M. Cadogan, D. H. Ryan and J. M. D. Coey, *Mater. Sci. Eng.*, *99* (1988) 143.
11 Z. Altounian and D. H. Ryan, *Mater. Sci. Eng.*, *99* (1988) 157.
12 Kh. Mulyukov, R. Z. Valiev, G. F. Korznikova and V. V. Stolyarov, *Phys. Status Solidi A*, *112* (1989) 137.
13 Y. Xu, W. B. Muir and Z. Altounian, *J. Magn. Magn. Mater.*, *82* (1989) 43.
14 A. Jha and H. A. Davies, *J. Non-cryst. Solids*, *113* (1989) 185.
15 M. T. Clavaguera-Mora, M. D. Baró, S. Suriñach and N. Clavaguera, *J. Mater. Res.*, *5* (1990) 1201.
16 S. Suriñach, M. D. Baró, M. T. Clavaguera-Mora and N. Clavaguera, *J. Non-Cryst. Solids*, *58* (1983) 209.
17 G. Schneider, E.-T. Henig, G. Petzow and H. H. Stadelmaier, *Z. Metallk.*, *77* (1986) 755.
18 S. Suriñach, M. D. Baró, J. A. Diego, N. Clavaguera and M. T. Clavaguera-Mora, *Acta Metall. Mater.*, *40* (1992) 37.
19 M. T. Clavaguera-Mora, M. D. Baró, S. Suriñach, J. A. Diego and N. Clavaguera, *IEEE Trans. Magn.*, *MAG-26* (1990) 2613.
20 A. Zaluska, Yan Xu, Z. Altounian, J. O. Ström-Olsen, R. Allen and G. Espérance, *J. Mater. Res.*, *6* (1991) 724.
21 C. R. Paik, M. Okada and M. Homma, *IEEE Trans. Magn.*, *MAG-26* (1990) 1730.